

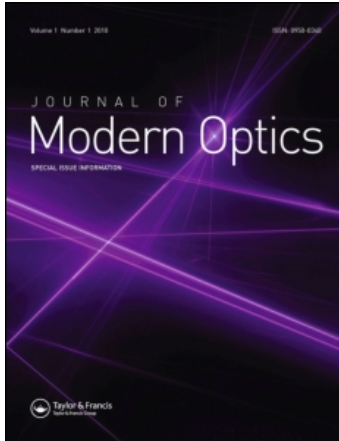
This article was downloaded by: [Duke University]

On: 17 May 2011

Access details: Access Details: [subscription number 931380209]

Publisher Taylor & Francis

Informa Ltd Registered in England and Wales Registered Number: 1072954 Registered office: Mortimer House, 37-41 Mortimer Street, London W1T 3JH, UK



## Journal of Modern Optics

Publication details, including instructions for authors and subscription information:

<http://www.informaworld.com/smpp/title~content=t713191304>

### Carrier-frequency dependence of a step-modulated pulse propagating through a weakly dispersive single narrow-resonance absorber

Heejeong Jeong<sup>a</sup>; Andrew M. C. Dawes<sup>a</sup>; Daniel J. Gauthier<sup>a</sup>

<sup>a</sup> Department of Physics, and The Fitzpatrick Institute for Photonics, Duke University, Durham, North Carolina 27708, USA

First published on: 18 April 2011

**To cite this Article** Jeong, Heejeong , Dawes, Andrew M. C. and Gauthier, Daniel J.(2011) 'Carrier-frequency dependence of a step-modulated pulse propagating through a weakly dispersive single narrow-resonance absorber', Journal of Modern Optics, 58: 10, 865 – 872, First published on: 18 April 2011 (iFirst)

**To link to this Article:** DOI: 10.1080/09500340.2011.575961

**URL:** <http://dx.doi.org/10.1080/09500340.2011.575961>

## PLEASE SCROLL DOWN FOR ARTICLE

Full terms and conditions of use: <http://www.informaworld.com/terms-and-conditions-of-access.pdf>

This article may be used for research, teaching and private study purposes. Any substantial or systematic reproduction, re-distribution, re-selling, loan or sub-licensing, systematic supply or distribution in any form to anyone is expressly forbidden.

The publisher does not give any warranty express or implied or make any representation that the contents will be complete or accurate or up to date. The accuracy of any instructions, formulae and drug doses should be independently verified with primary sources. The publisher shall not be liable for any loss, actions, claims, proceedings, demand or costs or damages whatsoever or howsoever caused arising directly or indirectly in connection with or arising out of the use of this material.

## Carrier-frequency dependence of a step-modulated pulse propagating through a weakly dispersive single narrow-resonance absorber

Heejeong Jeong<sup>\*†</sup>, Andrew M.C. Dawes<sup>‡</sup> and Daniel J. Gauthier

*Department of Physics, and The Fitzpatrick Institute for Photonics, Duke University, Durham, North Carolina 27708, USA*

*(Received 2 February 2011; final version received 24 March 2011)*

We observe interference between the optical precursors and the main signal for small optical depth  $\alpha_0 L \sim 1$ , in which the main signal cannot be entirely absorbed. Since the main signal oscillates at the carrier frequency of the input pulse and precursors oscillate at medium resonance frequency, in our case carrier frequency dependence of the total transmitted field is observed as a form of modulation patterns oscillating at the detuning frequency. To distinguish between the Sommerfeld and Brillouin precursors for the case of weakly dispersive off-resonance medium, we utilize asymptotic precursor theory under the assumption of small detuning.

**Keywords:** optical precursors; anomalous dispersion; cold atoms

### 1. Introduction

Many modern optical technologies, such as optical communication and medical imaging, require an understanding of how optical pulses propagate through a dispersive medium. Recently, the advent of methods for tailoring the dispersion of materials enables exquisite control of pulse propagation characteristics. For example, it is now possible to achieve an exceedingly slow or fast group velocity  $v_g$  compared with the speed of light in vacuum  $c$  for pulses of light propagating through a gas of atoms [1]. The achievement of slow and fast light has triggered fundamental questions about the information velocity as it relates to causality in Einstein's special theory of relativity. Over the past decade, researchers have proposed that encoding information on a pulse is related to non-analytic points. Because it is predicted that non-analytic points travel at  $c$ , it follows that the information velocity is also equal to  $c$  [2–4]. Stenner and colleagues confirmed this in both slow- [5] and fast-light experiments [6], where they encoded one bit of information on a pulse by rapidly changing the pulse intensity. By tracking when it is first possible to identify the bit, they showed that the information velocity is equal to  $c$  regardless of the dispersive properties of the medium.

It is generally believed that the rapid change of intensity on a pulse creates optical precursors [7–10], the transient behavior of the propagated field. In the

experiment by Stenner et al. [5,6], however, it was difficult to distinguish the precursors from the rest of the pulse because the rapid change in pulse intensity occurred in the middle of a time-dependent pulse waveform. To address this shortcoming, experiments need to be conducted that clearly tests for the existence of optical precursors occurring at the front of a step-modulated input pulse. We reported our first direct observation of long-lived optical precursors in [11] for the case when the carrier frequency of the pulse  $\omega_c$  was equal to the material resonance frequency  $\omega_0$ . The measurement was facilitated by extending the time scale of the precursors up to the order of tens of nanoseconds using a narrow-resonance absorber consisting of cold potassium atoms contained in a magneto-optical trap (MOT). Since then, optical precursors were predicted [12–14] and observed [15,16] in an electromagnetically-induced transparency (EIT). These series of studies, however, mostly focus on the case of an on-resonance and optically matured medium. Even for the recent study of an off-resonance precursor compared with the free induction decay [17], Sommerfeld and Brillouin precursors could not be distinguished.

In this paper, we describe our direct observation of interference between optical precursors and the main signal as we tune the carrier frequency from the two-energy-level cold atomic system. We will explain how the carrier frequency detuning is able to change the shape of the transmitted pulse, especially for an

\*Corresponding author. Email: jhj413@gmail.com

†Current address. Samsung Advanced Institute of Technology, Giheung, South Korea

‡Current address. Physics Department, Pacific University, Forest Grove, OR, USA

off-resonance and optically thin medium. To study this subject and identify optical precursors, we extend the asymptotic theory for on-resonance [18] to the case of off-resonance excitation ( $\omega_c \neq \omega_0$ ). We describe the experimental details in Section 2 to increase the duration of the optical precursor and the amplitude, which allows us to detect them directly using a standard experimental apparatus. The experimental results are described in Section 3 including interference between optical precursors and the main signal for the off-resonance case. In Sections 4.1 and 4.2, we compare our experimental observations to two different theories. One is based on an asymptotic analysis of the optical wave equation and a classical model of the dielectric, where the asymptotic analysis takes advantage of the fact that the material is weakly dispersive and has a narrow resonance [11]. The other is based on an analytic solution of the pulse propagation equations under the narrow-resonance, dilute-gas approximation, an approach commonly used by the quantum optics community [19]. From these analyses, we identify features of the experimentally observed propagated field that correspond to the composition of the Sommerfeld and the Brillouin precursors.

## 2. Experiments

To directly measure optical precursors, three steps are used. The experimental set-up is schematically shown in Figure 1. First, we prepare a cloud of cold potassium ( $^{39}\text{K}$ ) atoms to obtain a dielectric medium with a narrow resonance, which is the key to extending the precursor duration (Stage 1 in Figure 2). The cold atoms are optically pumped into one of the ground states of the potassium  $4S_{1/2}$  state ( $F=1$ ), thereby preparing essentially a single-resonance Lorentz dielectric (Stage 2 in Figure 2). Once the atoms are optically pumped, we send a weak-intensity, step-modulated pulse (carrier frequency  $\omega_c$ ) through the medium and measure the intensity of the transmitted pulse. In this section, we give further details of each experimental step.

### 2.1. Stage 1: preparation of a narrow resonance medium

To achieve a narrow-resonance, we use a vapor-cell magneto-optic trap [20]. The magneto optic-trap for neutral potassium atoms ( $^{39}\text{K}$ ) is realized using laser beams tuned to the  $4S_{1/2} \leftrightarrow 4P_{3/2}$  transition ( $D_2$  transition, 767-nm transition wavelength) and anti-Helmholtz coils. The trapped atoms have a temperature of  $\sim 400 \mu\text{K}$  measured by the release-and-recapture method [21]. At such cold temperatures, the resonance linewidth becomes of the order of the natural

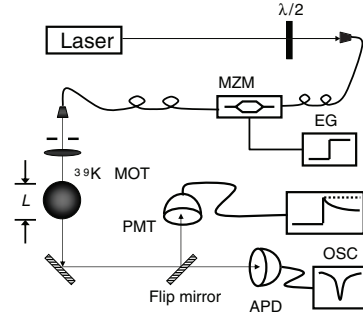


Figure 1. Experimental setup. EG: Edge generator, OSC: oscilloscope, APD: avalanche photodiode, PMT: photo multiplier tube, MZM: Mach-Zehnder modulator.

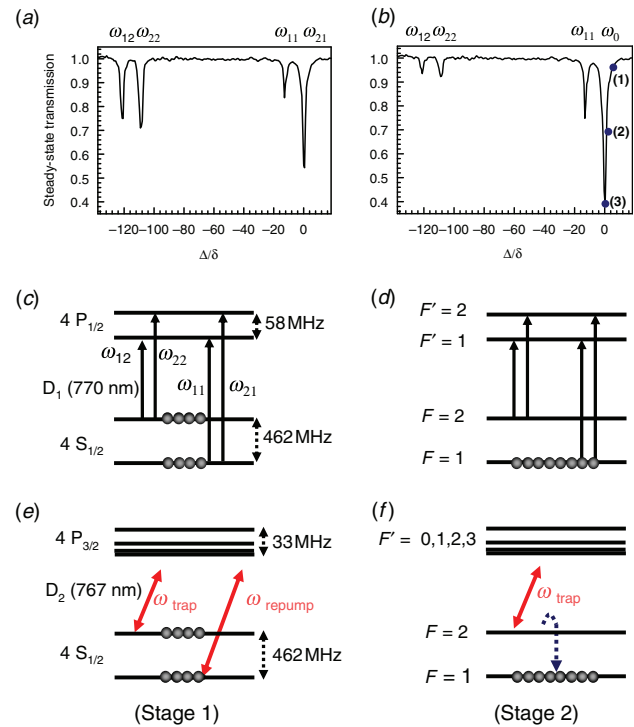


Figure 2. Transmission of a weak probe beam whose frequency is scanned through the four resonance peaks of the potassium  $D_1$  transition for the case of (a) both MOT beams on for  $80 \mu\text{s}$ , and (b) optical pumping into  $F=1$  state with trapping beam off for  $20 \mu\text{s}$ . Energy level diagrams of the  $D_1$  transition and population distribution in the ground states are shown in (c) and (d), explaining the origin of the four resonances shown in (a) and the two resonances shown in (b), respectively. Energy level diagrams of the  $D_2$  transition and population distribution in the ground states, are shown in (e) and (f) to illustrate the process of optical pumping. (The color version of this figure is included in the online version of the journal.)

linewidth (full width at half maximum)  $2\delta/2\pi = 1/2\pi t_{sp} \sim 6 \text{ MHz}$ , where  $t_{sp}$  is the spontaneous decay time of  $^{39}\text{K}$ . This width is much narrower than the resonance width of a Doppler-broadened potassium vapor at room temperature, which is typically  $800 \text{ MHz}$ .

The diameter of the MOT, which we take to be the length  $L$  of the medium, is determined to be in the range of  $\sim 1\text{--}2$  mm by measuring the  $1/e$  of the fluorescence of the MOT. The atomic number density is  $\sim 1\text{--}2 \times 10^{10} \text{ cm}^{-3}$  by measuring the absorption of a weak continuous-wave probe beam passing through the MOT.

The optical precursor experiment is conducted on the  $4S_{1/2} \leftrightarrow 4P_{1/2}$  transition ( $D_1$  transition, 770-nm transition wavelength), as shown in Figure 2(c) and (d). At the  $D_1$  transition, there are two ground states ( $F=1, 2$ ) and two excited states ( $F'=1, 2$ ). The corresponding four resonance peaks are denoted as  $\omega_{FF'}$ , where  $F'F$  denotes the  $4S_{1/2}(F) \leftrightarrow 4P_{1/2}(F')$  transition, as seen in Figure 2(c). At Stage 1, the two MOT beams (tuned near the  $D_2$  transition) are on, and the ground states are equally populated so that the absorption from the ground states to the excited states is well balanced, as shown in Figure 2(a), (c) and (e). As discussed in the next section,  $\omega_{21}$  will be treated as a single resonance peak. Therefore, we let the resonance frequency of the single-Lorentz medium  $\omega_0 \equiv \omega_{21}$  in this paper.

## 2.2. Stage 2: preparation of a single-Lorentz dielectric

To obtain a single-resonance Lorentz medium, we optically pump the atoms into one of the ground states  $4S_{1/2}(F=1)$ . To achieve optical pumping, the repumping beam (red detuned from  $4S_{1/2}(F=1) \leftrightarrow 4P_{3/2}$  transition) is repeatedly switched off for  $20 \mu\text{s}$  so that the remaining trapping beam optically pumps the atoms out of the  $F=2$  state and into the  $F=1$  state (Figure 2(f)). The repumping beam is then turned back on for  $80 \mu\text{s}$ , returning to Stage 1 (Figure 2(e)). Once in this state, the optical precursor experiment is conducted and the process is repeated.

The optical pumping time interval of  $20 \mu\text{s}$  is chosen to balance two conditions. One is to have enough time for the atomic states to reach equilibrium after optical pumping and to perform the optical precursor experiment. At the same time, we need to keep the total number of atoms constant in the trap during the optical pumping time.

After optical pumping, approximately 88% of the atoms are in the  $F=1$  state, leading to a suppression of resonances  $\omega_{12}$  and  $\omega_{22}$ , and enhancement of resonances  $\omega_{11}$  and  $\omega_0 = \omega_{21}$ , as seen in Figure 2(b). The difference in the heights of resonances  $\omega_{11}$  and  $\omega_0$  is due to differences in the corresponding dipole matrix elements. Resonance  $\omega_0$  is well isolated from resonance  $\omega_{11}$  (its width is much narrower than the spacing between the resonances) and we will use it to approximate a single-resonance Lorentz dielectric.

The properties of a single-resonance Lorentz dielectric are characterized by measuring the resonance linewidth  $\delta$  and the line-center absorption coefficient  $\alpha_0$  of the absorption peak near  $\omega_{21} = \omega_0$ , as shown in Figure 2(b). From the measurements of the frequency-dependent steady-state probe-laser-beam transmission  $T$  at line center (Figure 2(b)), we determine the half-width at half-maximum  $\delta$  and line-center absorption coefficient  $\alpha_0$ . From the measured values, we determine  $\alpha_0$  through Beer's Law  $T = \exp[-\alpha_0 L]$ , and a Lorentzian-like resonance with a width  $2\delta/2\pi \sim 9.6$  MHz (full width half maximum), which is broader than the 6-MHz natural linewidth. The broadened linewidth consists of residual Doppler broadening ( $< 1$  MHz), Zeeman splitting arising from the magnetic field gradient ( $\sim 2\text{--}3$  MHz), and the laser linewidth ( $\sim 200$  kHz). Because the time scale of precursor decay is of the order of  $1/2\delta$ , as we discuss later, the estimated precursor time scale is  $1/2\delta \sim 26$  ns.

Experimental measurements are obtained for a single value of the on-resonance absorption path length, set by adjusting the intensities of cooling and trapping laser beams. At their maximum intensity ( $\sim 33 \text{ mW/cm}^2$ ), we achieve an atomic number density of  $1.2 \times 10^{10} \text{ cm}^{-3}$  and a propagation length  $L = 0.20$  cm, resulting in a transmission of  $T = 0.36$ , corresponding to  $\alpha_0 = 5.14 \text{ cm}^{-1}$ ,  $\alpha_0 L = 1.03$ . With the trapping beams off, there are no trapped atoms and the transmitted pulse is identical to the incident pulse, which serves as a reference.

## 2.3. Stage 3: step modulated pulse propagation

The next stage is to pass a step-modulated pulse through the medium, and measure the temporal evolution of transmitted pulse intensity  $T(z, t)$ , where the  $z$  is the medium depth, and  $\tau = t - z/c$  is the retarded time. The incident pulse is created by passing a weak continuous-wave laser (frequency  $\omega_c$ ) through a 20-GHz-bandwidth Mach-Zehnder modulator (MZM, EOSpace, Inc.) driven by an electronic edge generator (Data Dynamics, Model 5113) whose edge is steepened using a back recovery diode (Stanford Research Systems, Model DG535), resulting in an edge with a rise time of  $\sim 100\text{--}200$  ps. The peak intensity of the pulse is  $\sim 64 \mu\text{W/cm}^2$ , which is much less than the saturation intensity of the transition ( $\sim 3 \text{ mW/cm}^2$ ). A weak-intensity incident pulse is important to avoid nonlinear optical phenomenon. The pulse is detected with a fast-rise-time (0.78 ns) photomultiplier tube (PMT, Hamamatsu, Model H6780-20) and the resulting electrical signal is measured with a 1-GHz analog bandwidth digital oscilloscope (Tektronix, Model TDS 680B). In the absence of the atoms, we measure an edge

rise time (10–90%) of  $\sim 1.7$  ns for the complete system, corresponding to a bandwidth of  $\sim 206$  MHz. This time is short in comparison to the expected duration of the precursors.

To calibrate  $\omega_c$ , we measure its detuning with respect to the atomic resonance frequency via the steady-state transmission spectrum. From knowledge of the hyperfine splitting of the  $4P_{1/2}$  state (58 MHz), we calibrate the horizontal axis of the scan. The detuning  $\Delta = \omega_c - \omega_0$  is then determined by comparing the steady-state transmission spectrum with the value of the long-time intensity of the transmitted pulse in our transient experiments with values  $\Delta_{(1)} = 27.1^{+3.2}_{-2.1}$  MHz,  $\Delta_{(2)} = 5.3^{+0.5}_{-0.4}$  MHz, and  $\Delta_{(3)} = 0^{+2.3}_{-2.3}$  MHz as indicated in Figure 2. The errors associated with these measurements arise from our mapping of transmission to frequency and are asymmetric due to the fact that the slope of the curve is different at each point.

### 3. Experimental results

The black solid lines in Figure 3 show the measured transmitted pulse intensities  $T(z, \tau)$  for different carrier frequencies  $\omega_c$  tuned near the  $4S_{1/2}(F=1) \leftrightarrow 4P_{1/2}(F=2)$  transition.

Figure 3(a) (point (1) in Figure 2(b)) shows the case when  $\Delta = \Delta_{(1)} \sim 5\delta$ . It is seen that the transient transmitted intensity immediately reaches  $\sim 90\%$  of the incident pulse height. The transmitted intensity is ideally 100%, but it is reduced to 90% by the 206-MHz electronics bandwidth. The transmission intensity oscillates with a modulation frequency of approximately  $\Delta$  and its inverse corresponds to a modulation period of  $\sim 40$  ns. The amplitude of oscillations then decays to the steady-state value, which obeys Beer's law. The time scale for the transmitted intensity to reach its steady-state value is similar to that observed for  $\Delta = 0$ , as shown in Figure 3(c), which implies that the precursor time scale only depends on  $\delta$  for the case of small  $\alpha_0 L \sim 1$ . As discussed later, the oscillation of the envelope results from the interference between the precursors oscillating at  $\omega_0$  and the main signal oscillating at  $\omega_c$ . Consequently, the modulation patterns decay at a rate of  $\delta$ .

For the case of a moderately blue-shifted carrier frequency ( $\Delta = \Delta_{(2)} \sim \delta$ ), as shown in Figure 3(b) (point (2) in Figure 2(b)), the initial transmission also rises immediately to  $\sim 90\%$ , and decays to the steady state with a slower oscillation than the case for  $\Delta = \Delta_{(1)} \sim 5\delta$ .

Note that, for the case of  $\Delta = \Delta_{(1)} \sim 5\delta$ , shown in Figure 3(a),  $T(z, \tau)$  oscillates after the peak until it reaches its steady-state value. During the oscillation, it attains values greater than unity. This phenomenon can be explained as follows. When the medium

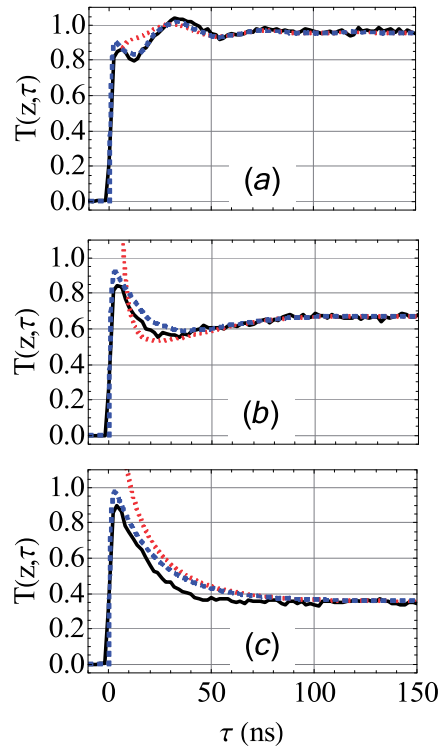


Figure 3. Experimentally obtained transient transmission intensity (black solid lines) compared with two theoretical analysis: the asymptotic analysis (Equations (8)–(9) and Equation (10), red dotted lines), and the weakly dispersive narrow resonance (Equations (13)–(17) and Equation (17), blue dashed lines). Transient transmission taken near the  $4S_{1/2}(F=1) \leftrightarrow 4P_{1/2}(F=2)$  transition for (a)  $\Delta = \Delta_{(1)} \sim 5\delta$ ; (b)  $\Delta = \Delta_{(2)} \sim \delta$ ; and (c)  $\Delta = \Delta_{(3)} \sim 0$ . (The color version of this figure is included in the online version of the journal.)

polarization starts to react to the incident light, the polarization is out of phase with the incident field, indicating that the energy of incident light is stored temporarily by the medium. The stored energy is re-emitted afterward at a later time, causing greater than unity transmission.

### 4. Analysis: two approaches

The experimental results described in the previous section clearly demonstrate transient behavior, yet it is not clear which part of the waveform can be attributed to the precursor or to the main signal parts of the field.

Consider a dispersive medium consisting of a collection of Lorentz oscillators possessing a single resonance. The refractive index for this medium (or a collection of two-level atoms) is given by

$$n(\omega) = \sqrt{\epsilon(\omega)} = \sqrt{1 - \frac{\omega_p^2}{\omega^2 - \omega_0^2 + 2i\omega\delta}}, \quad (1)$$

where  $\epsilon(\omega)$  is a linear frequency-dependent dielectric constant,  $\omega_p$  is the plasma frequency,  $\delta$  is the resonance absorption linewidth (HWHM), and  $\omega_0$  is the atomic resonance frequency. The plasma frequency  $\omega_p$  quantifies the strength of the resonance and is related to the line-center absorption coefficient through the relation  $\alpha_0 \simeq \omega_p^2/2\delta c$ , which is only true for small  $\omega_p$ . The temporal evolution of the transmitted scalar electric field  $E(z, t)$  at a medium penetration depth  $z$  in the half-space  $z > 0$  can be written as an integral representation given by

$$E(z, t) = \frac{1}{2\pi} \int_{ia-\infty}^{ia+\infty} E(0, \omega) e^{i(k(\omega)z - \omega t)} d\omega, \quad (2)$$

where  $a$  is a positive definite real constant and

$$E(0, \omega) = \int_{-\infty}^{+\infty} E(z=0_+, t) e^{i\omega t} dt \quad (3)$$

is the temporal Fourier spectrum of the incident beam just inside the dispersive medium. The complex wave number  $k(\omega)$  is related to the complex index of refraction through  $k(\omega) = \omega n(\omega)/c$ . If the incident beam is taken as a step-modulated sinusoidal electric field of the form  $E(z=0, t) = E_0 \Theta(t) e^{-i\omega_c t}$ , where  $\Theta(t)$  is the Heaviside unit step function with spectrum  $i/\omega$  for  $\Im\{\omega\} > 0$ , then the complex transmitted field is given by

$$E(z, t) = \frac{E_0}{2\pi} \left\{ \int_{ia-\infty}^{ia+\infty} \frac{i}{\omega - \omega_c} e^{z\phi(\omega, t)/c} d\omega \right\}. \quad (4)$$

Here, the complex function  $\phi(\omega, t)$  appearing in Equation (4) is defined as  $\phi(\omega, t) \equiv i\omega[n(\omega) - ct/z]$ . Equation (4) is the starting point of the theories.

The transmitted field, expressed in integral form in Equation (4), consists of two parts: transient responses (the precursors) and steady-state responses (the main signal). However, this equation has no exact analytic solution. To identify each part, we will discuss two theoretical approaches to solve Equation (4) and compare their predictions to our data.

#### 4.1. The numerical asymptotic method

Equation (4) for the total transmitted field can be evaluated using the saddle-point method, which is valid in the limit when a distance into the medium,  $z$ , is greater than one optical penetration depth  $\alpha_0^{-1}$  [10]. In the asymptotic regime, the integral has a non-zero value when it is evaluated near the extremum value (saddle-points) of the phase  $z\phi(\omega, t)/c$ . The extremum values are the so-called saddle-points  $\omega_{sp}$ , which are solutions to the first derivative with respect to  $\omega$ ,

$\phi'(\omega_{sp}, t) \equiv \partial\phi(\omega, t)/\partial\omega|_{\omega_{sp}} = 0$ . At each  $\omega_{sp}$ , the contribution to integral Equation (4) is given by

$$E_{\omega_{sp}}(z, t) = \frac{iE_0}{\sqrt{2\pi(\omega_{sp} - \omega_c)}} \frac{e^{z\phi(\omega_{sp}, t)/c + i\psi}}{|z\phi''(\omega_{sp}, t)/c|}, \quad (5)$$

where  $\psi$  is the angle of steepest decent [22], and  $\phi''(\omega_{sp}, t) \equiv \partial^2\phi(\omega_{sp}, t)/\partial\omega^2$ , the second derivative with respect to  $\omega$ .

For  $\Delta=0$  and any optical depth  $\alpha_0 L$ , the two classes of saddle points  $\omega_{sp}^{\pm}$  are analytically evaluated (see [15,23]) as

$$\omega_{sp}^{\pm} = \omega_0 - i\delta \pm \sqrt{p/\tau}, \quad (6)$$

where  $p \equiv \omega_p^2 z/4c = \alpha_0 \delta z/2$ . These saddle points are related to the two types of transient responses known as Sommerfeld [ $E_S(z, t)$ ] and Brillouin precursors [ $E_B(z, t)$ ] [12]. The total Sommerfeld–Brillouin precursors,  $E_{SB}(z, t) = E_S(z, t) + E_B(z, t)$ , take the form of a modulated cosine or Bessel function [11,13,15,23]. For off-resonance case  $\Delta \neq 0$ , however, such analytic expressions of each  $E_S(z, t)$  and  $E_B(z, t)$  are absent.

To obtain  $E_S(z, t)$  and  $E_B(z, t)$  separately, for the first time in the optically thin  $\alpha_0 L \sim 1$  and off-resonance  $\Delta \neq 0$  regime, we utilize the numerical asymptotic theory for  $\alpha_0 L \sim 1$  and  $\Delta=0$  [18] by substituting  $\omega_0$  with  $\omega_c$  based on the assumption of the small detuning of the order of  $\delta$ .

The location of the saddle-points and the amplitudes of each precursor are evaluated numerically. We set the variable of integration as  $\xi \equiv i(\omega + i\delta)$ , which is shifted by  $-\delta$  from the imaginary axis of complex frequency  $\omega$  and rotated by  $90^\circ$  [18]. The phase of the integrand is thus simplified as  $z\phi(\omega, t)/c \equiv z(\xi + \delta)$  [ $R_1/R_2 - ct/z$ ]/ $z_0$ , and the saddle-point equation is now given by

$$R_1^3 R_2 ct/z - R_1^2 R_2^2 + (R_2^2 - R_1^2)\xi(\xi + \delta)|_{\xi_{sp}} = 0, \quad (7)$$

where  $z_0 \equiv \omega_0/c$ ,  $R_1 \equiv \sqrt{(\xi^2 + \omega_0^2 - \delta^2)/\omega_0^2}$ , and  $R_2 \equiv \sqrt{(\xi^2 + \omega_0^2 + \omega_p^2 - \delta^2)/\omega_0^2}$ . Using the numerically obtained values of four saddle points  $\xi_{sp}^{\pm}$  ( $\xi_S^{\pm}$  and  $\xi_B^{\pm}$ ), we then evaluate the non-vanishing complex field envelope  $A(z, t)$  using Equation (5) as

$$A_S(z, t) = \sum_{\xi_S^{\pm}} \frac{\mp E_0}{\sqrt{2\pi}} \frac{e^{\frac{z}{c}\phi(\xi_S^{\pm}(z, t), t) - \frac{1}{2}Arg[\phi''(\xi_S^{\pm}(z, t))]} }{(\xi_S^{\pm}(z, t) + \delta - i\omega_c) \sqrt{z_0} |\phi''(\xi_S^{\pm}(z, t))|}, \quad (8)$$

$$A_B(z, t) = \sum_{\xi_B^{\pm}} \frac{\mp E_0}{\sqrt{2\pi}} \frac{e^{\frac{z}{c}\phi(\xi_B^{\pm}(z, t), t) - \frac{1}{2}Arg[\phi''(\xi_B^{\pm}(z, t))]} }{(\xi_B^{\pm}(z, t) + \delta - i\omega_c) \sqrt{z_0} |\phi''(\xi_B^{\pm}(z, t))|}, \quad (9)$$

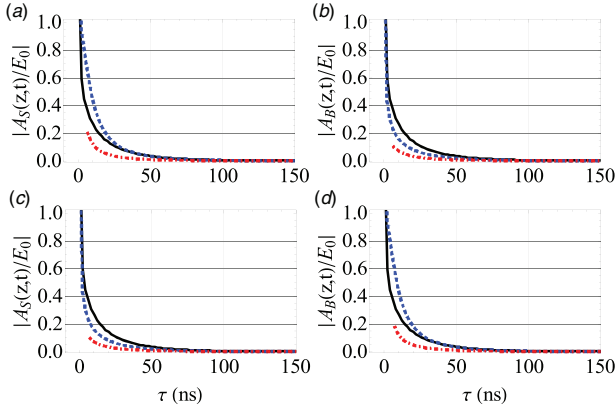


Figure 4. Value of the field envelopes obtained by using the numerical asymptotic theory given by Equations (8)–(9). The Sommerfeld precursors  $|A_S(z, t)/E_0|$  are evaluated for (a)  $\Delta > 0$ , and (c)  $\Delta < 0$ , and the Brillouin precursors  $|A_B(z, t)/E_0|$  are evaluated for (b)  $\Delta > 0$ , and (d)  $\Delta < 0$ . In each figure, there are three cases for  $\Delta = 0$  (black solid lines),  $|\Delta| \sim \delta$  (blue dashed lines), and  $|\Delta| \sim 5\delta$  (red dash-dot lines). (The color version of this figure is included in the online version of the journal.)

where  $\sum_{\xi^\pm}$  indicates the summation over each case of  $\xi^+$  on the  $\Im(\xi) > 0$  plane and  $\xi^-$  on the  $\Im(\xi) < 0$  plane. Note that, for the resonant-carrier case, the Sommerfeld precursor (Equation (8)) and the Brillouin precursor (Equation (9)), shown in Figure 4 separately, can be simplified and the sum of the two is approximated as a Bessel or cosine function, as previously mentioned.

Blue lines denote the case of  $|\Delta| \sim \delta$ , and the red lines indicate the case of  $|\Delta| \sim 5\delta$ . For  $\Delta = 0$ , both precursors have the same amplitude (black lines). When the carrier frequency  $\omega_c$  is higher than the medium resonance  $\omega_0$ , i.e.  $\Delta > 0$ , the amplitude of the Sommerfeld precursor (high frequency transient) (Figure 4(a)) is larger than the amplitude of the Brillouin precursor (Figure 4(b)). For  $\Delta < 0$ , on the other hand, the Brillouin precursor (the low frequency transient) (Figure 4(d)) dominates over the Sommerfeld precursor (Figure 4(c)). Note that  $|A_S(z, t)/E_0|$  for  $\Delta > 0$  case (Figure 4(a)) is the same as  $|A_B(z, t)/E_0|$  for  $\Delta < 0$  (Figure 4(d)) due to the symmetry in the detuning parameters. The total precursor amplitudes  $|A_{SB}(z, t)/E_0|$  are shown in Figure 5(e) for different  $\Delta$ .

The saddle points are not the only source of a non-zero contribution to the integral. Note that the saddle points contribute the most when  $1/(\omega - \omega_c)$  varies slowly compared with  $\exp[z\phi(\omega, t)/c]$ . For  $\omega = \omega_c$ , however,  $1/(\omega - \omega_c)$  has a singular point (pole), where it diverges rapidly. The pole contribution to the integral is related to the steady-state response of the

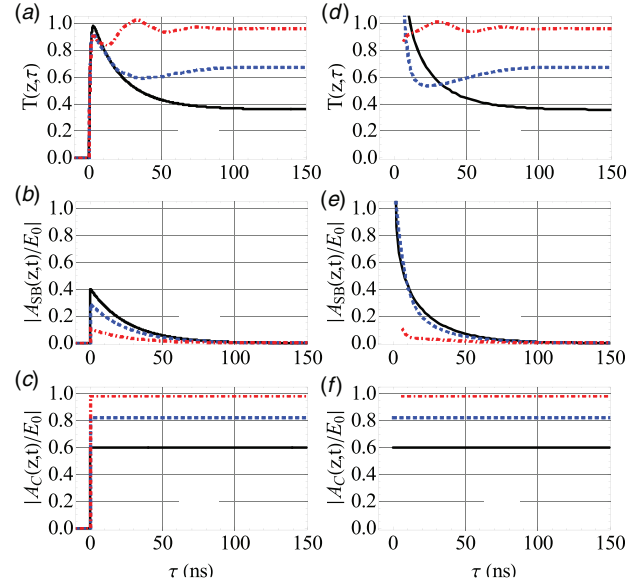


Figure 5. Comparison of two theories: the weakly dispersive narrow resonance case ((a)–(c), Equations (13)–(15)) and asymptotic theory ((d)–(f), Equations (8)–(9) and Equation (10)). The total transmission  $T(z, t)$  (a), (d), the envelopes of total precursors  $|A_{SB}(z, t)/E_0|$  (b), (e), and the main signal  $|A_C(z, t)/E_0|$  (c), (f) are evaluated for our experimental conditions. In each figure, the red dash-dot line denotes  $\Delta \sim 5\delta$ , the blue dashed line indicates  $\Delta \sim \delta$ , and the black solid line denotes  $\Delta \sim 0$ . (The color version of this figure is included in the online version of the journal.)

medium to the incident field [10]. The steady-state response is known as the main signal (see Figure 5(f))

$$A_C(z, t) = 2\pi i \text{Res}(\xi = i\omega_c - \delta), \quad (10)$$

which is identical to the steady-state term predicted by the analytic expression for the weakly dispersive narrow-resonance case discussed in the next section.

The field envelope is expressed as  $A(z, t)$ , such that  $E(z, t) = A(z, t)e^{-i\omega_c t}$ ,  $E_{S[B]}(z, t) = A_{S[B]}(z, t)e^{-i\omega_c t}$ , and  $E_C(z, t) = A_C(z, t)e^{-i\omega_0 t} = A_C(z, t)e^{i\Delta t}e^{-i\omega_c t}$ . To compare this theory with our experimental data, the normalized total transmitted intensities  $T(z, t) = |E(z, t)/E_0|^2$  are evaluated from Equations (8)–(10), and plotted in Figure 3 (red lines) and Figure 5(d). Near the front  $\tau = 0$ , inaccuracy become significant especially for small  $\alpha_0 L$  [23], but it has been quite improved compared with the large error that appeared in [11]. Besides, for our experimental parameters, the analysis is accurate when  $\tau \gg 64.7$  ns according to the validity of the asymptotic analysis [23]. Therefore, the asymptotic theory can be used for small  $\alpha_0 L$  and has confirmed our interpretation that the transients observed in our experiment consist of Sommerfeld and Brillouin precursors.

#### 4.2. Analytic expression for weakly dispersive, narrow-resonance case

In the previous section, although the accuracy near front ( $\tau=0$ ) remains the issue, Sommerfeld and Brillouin precursors are distinguished for arbitrary  $\Delta$  based on the asymptotic analysis. In this section, we compare the data to an analytic method accurately describing the transmitted amplitude  $E(z, t)$  consisting of a total transient contribution (the precursors,  $E_{SB}(z, t)$ ) and a steady-state contribution (the main signal,  $E_C(z, t)$ ) [24,25]. The modulation pattern for  $\Delta \neq 0$  will be described in total transmission intensity  $T(z, t)$ .

By assuming that the medium is weakly dispersive ( $\omega_p \ll \sqrt{8\delta\omega_0}$ ), has a narrow resonance ( $\delta \ll \omega_0$ ), and that the carrier frequency of the pulse is near the material resonance ( $\omega \approx \omega_0$ ), the index of refraction  $n(\omega)$  (Equation (1)) is approximately given as

$$n(\omega) \simeq 1 - \frac{1}{4} \frac{\omega_p^2}{\omega(\omega - \omega_0 + i\delta)}. \quad (11)$$

With this approximation, Equation (4) becomes

$$E(z, t) = \frac{iE_0}{2\pi} \int_{ia-\infty}^{ia+\infty} \frac{e^{-i\omega\tau - ip/(\omega - \omega_0 + i\delta)}}{\omega - \omega_0} d\omega, \quad (12)$$

where  $\tau \equiv t - z/c$ . Note that these assumptions are also used in the SVA approximation [24], with the additional step of assuming a slowly varying amplitude, which we do not assume here. Therefore, the assumptions used to obtain Equation (12) do not lead to the SVA approximation [23] but instead describe a ‘weakly dispersive, narrow-resonance (WDNR) assumption’. It is possible to obtain a simple analytic solution of Equation (12) by contour integration [24,25].

$$A(z, t) = E_0 \Theta(\tau) \left( e^{\frac{p}{i\Delta - \delta}} - e^{(i\Delta - \delta)\tau} \sum_{n=1}^{\infty} \left( \frac{\sqrt{p/\tau}}{i\Delta - \delta} \right)^n J_n(2\sqrt{p\tau}) \right), \quad (13)$$

$$A(z, t) = E_0 \Theta(\tau) e^{(i\Delta - \delta)\tau} \sum_{n=0}^{\infty} \left( \frac{-i\Delta + \delta}{\sqrt{p/\tau}} \right)^n J_n(2\sqrt{p\tau}), \quad (14)$$

$$A_C(z, t) = E_0 \Theta(\tau) e^{\frac{p}{i\Delta - \delta}}. \quad (15)$$

where Equation (13) (Equation (14)) should be used for  $\tau > p/|i\Delta - \delta|^2$  ( $\tau < p/|i\Delta - \delta|^2$ ). The first term of Equation (13) corresponds to the main signal  $E_C(z, t) = \Re[E_0 \Theta(\tau) e^{p/(i\Delta - \delta)} e^{-i\omega_c \tau}]$ . The amplitude of the main signal increases as the detuning  $\Delta$  increases because there is less absorption (see Figure 5(c)).

The second term is the sum of Sommerfeld and Brillouin precursors  $E_{SB}(z, t)$ , where the peak of the total precursor envelope decreases as the detuning increases (see Figure 5(b)).

For the case of an off-resonance carrier frequency ( $\Delta \neq 0$ ), the WDNR approximation (blue dashed lines in Figure 3) shows that the modulation of the total transmitted intensity depends on the detuning  $\Delta$  (see Figure 3(a)). This is because both precursor fields (the second term in Equation (13)) oscillate near the medium resonance frequency  $\omega_0 (= -\Delta + \omega_c)$ , while the main signal (first term) oscillates at the carrier frequency of the incident pulse  $\omega_c$ . The modulation pattern is also explained by the cross term  $E_{SB}(z, t) \times E_C(z, t)$  of  $T(z, t) = |E(z, t)/E_0|^2$  evaluated from Equations (13)–(15) as

$$\begin{aligned} T(z, t) = |E(z, t)/E_0|^2 &\simeq |E_{SB}(z, t)/E_0|^2 + |E_C(z, t)/E_0|^2 \\ &+ \frac{2p}{\sqrt{\Delta^2 + \delta^2}} \frac{J_1(2\sqrt{p\tau})}{\sqrt{p\tau}} e^{-\delta\tau - \delta p/(\Delta^2 + \delta^2)} \\ &\times \cos\left(\Delta\tau + \frac{\Delta p}{\Delta^2 + \delta^2} + \varphi(\Delta)\right) + \dots, \end{aligned} \quad (16)$$

where we have retained the dominant first term ( $n=1$ ) and dropped the higher order terms in Equation (13). The modulation frequency is  $\Delta/2\pi$ , as shown in Equation (16). Therefore, it is confirmed that the difference in frequencies between total precursors and the main signal gives rise to modulation of the total transmitted field intensity.

The modulation patterns in Figure 3 were also observed by Hamermesh et al. (figures 6–9 of [24]) when they studied the time-dependent emission of gamma rays propagating through an absorptive filter. They detuned the energy of the gamma rays from the resonant energy of the filter. (Note that, although their analysis is based on a single-sided decaying exponential input pulse, it can be modified to a step-modulated pulse when we set the exponent to zero.) They also observed transient non-exponential decay of resonantly filtered gamma rays, which might be another realization of precursors in electromagnetic pulse propagation.

The transmitted intensity measured in our experiment is smoothed out by the finite bandwidth of our measuring system. To take into account the finite rise time of the step-modulated pulse and detection system, we convolve the theoretically predicted intensity transmission function  $T(z, t)$  with the expression for a single-pole low-pass filter

$$\frac{dy(t)}{dt} = -\gamma_f [y(t) - T(z, t)], \quad (17)$$

where  $y(t)$  is the filtered transmission function and  $\gamma_f = 2\pi$  (206-MHz) is the 3-dB roll-off frequency in

rad/s. The filter reduces the transmission to  $\sim 95\%$  immediately after the front. The blue dashed lines in Figure 3 show our predictions of the low-pass-filtered intensity transmission function, which agree well with the experimental observations.

## 5. Discussion

Carrier frequency affects the propagating transient pulse only for the case of optically thin media, i.e.  $\alpha_0 L \sim 1$ , where the main signal cannot be entirely absorbed in a two-level system. This is because only the main signal oscillates at the carrier frequency  $\omega_c$  of the input pulse, and the frequencies of the precursors are determined by the medium characteristics, in our case,  $\omega_0$ . By having both the precursors and the main signal, we observe oscillatory modulations on the total transmitted pulse intensity and the modulation decay timescale inversely proportional to  $\delta$ . It is also interpreted as the interference between forced and free oscillation [26]. Note that this interference will disappear as one increases the optical depth to the point where the main signal is entirely absorbed. Thus, for the optically thick medium, the optical precursors are the only part of the signal that survive in transmission. In that case, the field envelope is dominated by the Bessel function and the time scale is inversely related to  $p = \alpha_0 L \delta / 2$  rather than  $\delta$ . Despite the similar phenomena, which have been observed as ‘coherent transient’ [19,24,27–30], the possibility of optical precursors was excluded until recently [14].

To distinguish between  $E_S(z, t)$  and  $E_B(z, t)$  numerically in the regime of  $\alpha_0 L \sim 1$  and  $\Delta \neq 0$ , simple modification of the existing theory [18] was performed based on the assumption of small detuning. A recent study combining free-induction decay and optical precursors [17] could not distinguish those two and, to our knowledge, we first identify each precursor in the regime of  $\alpha_0 L \sim 1$  and  $\Delta \neq 0$  to understand carrier frequency dependence of the transient pulse propagation.

## Acknowledgements

We gratefully acknowledge discussions of this research with Kurt Oughstun, Lucas Illing, Shengwang Du, and Ulf Österberg. This research was supported by the US NSF through Grant No. PHY-0139991.

## References

[1] Boyd, R.W.; Gauthier, D.J. In *Progress in Optics* 43: Wolf, E., Ed.; Elsevier: Amsterdam, 2002; Chapter 6.

- [2] Chiao, R.Y.; Steinberg, A.M. In *Progress in Optics XXXVII*: Wolf, E., Ed.; Elsevier: Amsterdam, 1997; pp 345–405.
- [3] Garrison, J.C.; Mitchell, M.W.; Chiao, R.Y.; Bolda, E.L. *Phys. Rev. Lett. A* **1998**, *245*, 19–25.
- [4] Parker, M.C.; Walker, S.D. *Opt. Commun.* **2004**, *229*, 23–27.
- [5] Stenner, M.D.; Gauthier, D.J.; Neifeld, M.A. *Phys. Rev. Lett.* **2005**, *94*, 053902.
- [6] Stenner, M.D.; Gauthier, D.J.; Neifeld, M.A. *Nature* **2003**, *425*, 695–698.
- [7] Brillouin, L. *Wave Propagation and Group Velocity*; Academic Press: New York, 1960.
- [8] Stratton, J.A. *Electromagnetic Theory*; McGraw-Hill: New York and London, 1941.
- [9] Jackson, J.D. *Electrodynamics*, 3rd ed.; Wiley: New York, 1999; pp 322–339.
- [10] Oughstun, K.E.; Sherman, G.C. *Electromagnetic Pulse Propagation in Causal Dielectrics*; Springer-Verlag: Berlin, 1994.
- [11] Jeong, H.; Dawes, A.M.C.; Gauthier, D.J. *Phys. Rev. Lett.* **2006**, *96*, 143901.
- [12] Jeong, H.; Du, S. *Phys. Rev. A* **2009**, *79*, 011802(R).
- [13] Jeong, H.; Du, S. *Opt. Lett.* **2010**, *35*, 124–126.
- [14] Macke, B.; Segard, B. *Phys. Rev. A* **2009**, *80*, 011803(R).
- [15] Wei, D.; Chen, J.F.; Loy, M.M.T.; Wong, G.K.L.; Du, S. *Phys. Rev. Lett.* **2009**, *103*, 093602.
- [16] Chen, J.F.; Jeong, H.; Feng, L.; Loy, M.M.T.; Wong, G.K.L.; Du, S. *Phys. Rev. Lett.* **2010**, *104*, 223602.
- [17] Chen, J.F.; Wang, S.; Wei, D.; Loy, M.M.T.; Wong, G.K.L.; Du, S. *Phys. Rev. A* **2010**, *81*, 033844.
- [18] LeFew, W.R. Unpublished Ph.D. dissertation, Duke University, Durham, NC, 2007.
- [19] Crisp, M.D. *Phys. Rev. A* **1970**, *1*, 1604–1611.
- [20] Wieman, C.; Flowers, G.; Gilbert, S. *Am. J. Phys.* **1995**, *63*, 317–330.
- [21] Chu, S.; Hollberg, L.; Bjorkholm, J.E.; Cable, A.; Ashkin, A. *Phys. Rev. Lett.* **1985**, *55*, 48–51.
- [22] Bleistein, N.; Handelsman, R.A. *Asymptotic Expansions of Integrals*; New York: Dover, 1986.
- [23] LeFew, W.R.; Venakides, S.; Gauthier, D.J. *Phys. Rev. A* **2009**, *79*, 063842.
- [24] Lynch, F.J.; Holland, R.E.; Hamermesh, M. *Phys. Rev.* **1960**, *120*, 513–520.
- [25] Aaviksoo, J.; Lippmaa, J.; Kuhl, J. *J. Opt. Soc. Am. B* **1988**, *5*, 1631–1635.
- [26] Jeong, H.; Osterberg, U.L. *Phys. Rev. A* **2008**, *77*, 021803(R).
- [27] Ségard, B.; Zemmouri, J.; Macke, B. *Europhys. Lett.* **1987**, *4*, 47–52.
- [28] Dudovich, N.; Oron, D.; Silberberg, Y. *Phys. Rev. Lett.* **2002**, *88*, 123004.
- [29] Varoquaux, E.; Williams, G.A.; Avenel, O. *Phys. Rev. B* **1986**, *34*, 7617–7640.
- [30] Rothenberg, J.E.; Grischkowsky, D.; Balant, A.C. *Phys. Rev. Lett.* **1984**, *53*, 552–555.